Electronic Supplementary Information (ESI) for

Controllable synthesis of N/Co-doped carbon from metal-organic framework for integrated solar vapor generation and advanced oxidation process

Panpan He, Huiying Bai, Zifen Fan, Liang Hao, Ning Liu, Bingyu Chen, Ran Niu*, Jiang Gong*

Key Laboratory of Material Chemistry for Energy Conversion and Storage, Ministry of Education, Semiconductor Chemistry Center, Hubei Key Laboratory of Material Chemistry and Service Failure, Hubei Engineering Research Center for Biomaterials and Medical Protective Materials, School of Chemistry and Chemical Engineering, Huazhong University of Science and Technology, Wuhan 430074, China.

*Corresponding authors.

E-mail addresses: niuran@hust.edu.cn (R. Niu); gongjiang@hust.edu.cn (J. Gong)

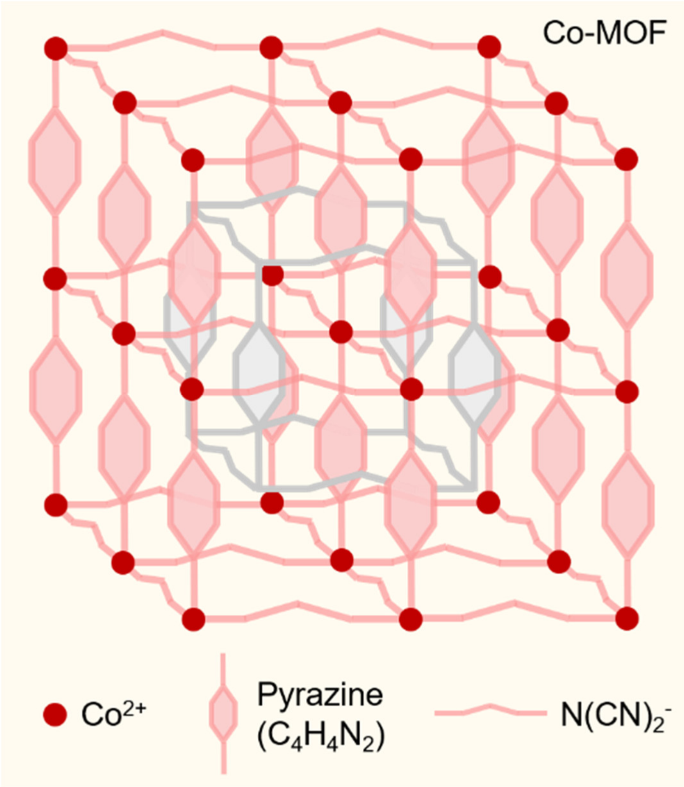

Fig. S1 Scheme for two interpenetrating related networks of Co-MOF (i.e., Co(dca)$_2$pyz, dca = dicyanamide = $N(CN)_2^-$, pyz = pyrazine = $C_4H_4N_2$).

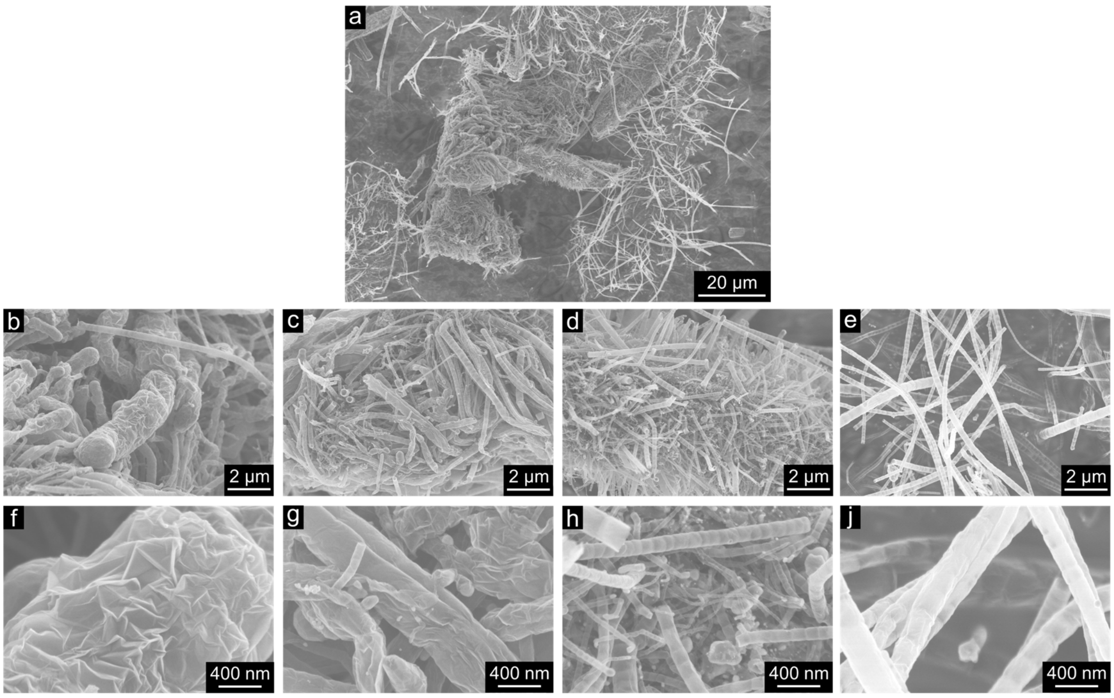

Fig. S2 SEM images of NC-650 obtained by calcination of Co-MOF at 650 °C: (a) low magnification; (b and f) thick wrinkled microrod; (c and g) thin wrinkled microrod; (d and h) short bamboo-like carbon tube; (e and f) long bamboo-like carbon tube.

Note: There is a sudden change of morphology for the carbon material from 600 to 700 °C. As shown in Fig. 2 in the manuscript, NC-500/600 exhibit the microrod morphology, while NC-700/800 present the bamboo-like carbon tube morphology. Furthermore, we studied the morphology of NC-650 derived from the intermediate temperature (650 °C). As shown in Fig. S2, NC-650 consists of the mixture of thick or thin wrinkled microrod as well as short or long bamboo-like carbon tube. In other word, the structure of NC-650 is complex and uneven. We infer that the carbon nanotube might grow from the microrod matrix, and the surface-folded microrod may be decomposed from the initially grooved microrod. For the higher temperature (e.g., 700 °C), the microrod completely converts into wrinkled bamboo-like carbon tube. Hence, the calcination temperature is optimized as 500, 600, 700 and 800 °C in this work.

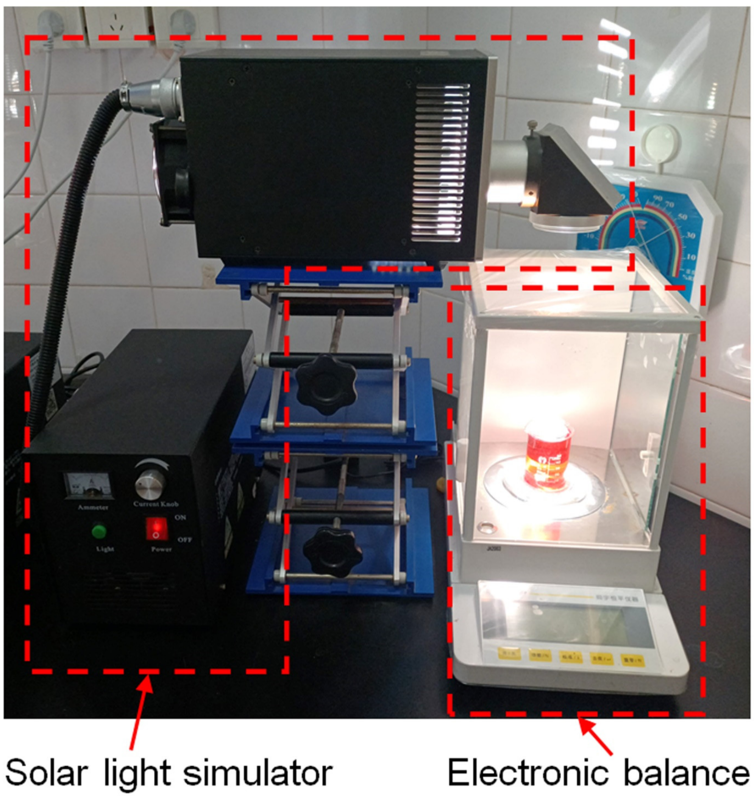

Fig. S3 Photograph of interfacial solar vapor generation system in this work.

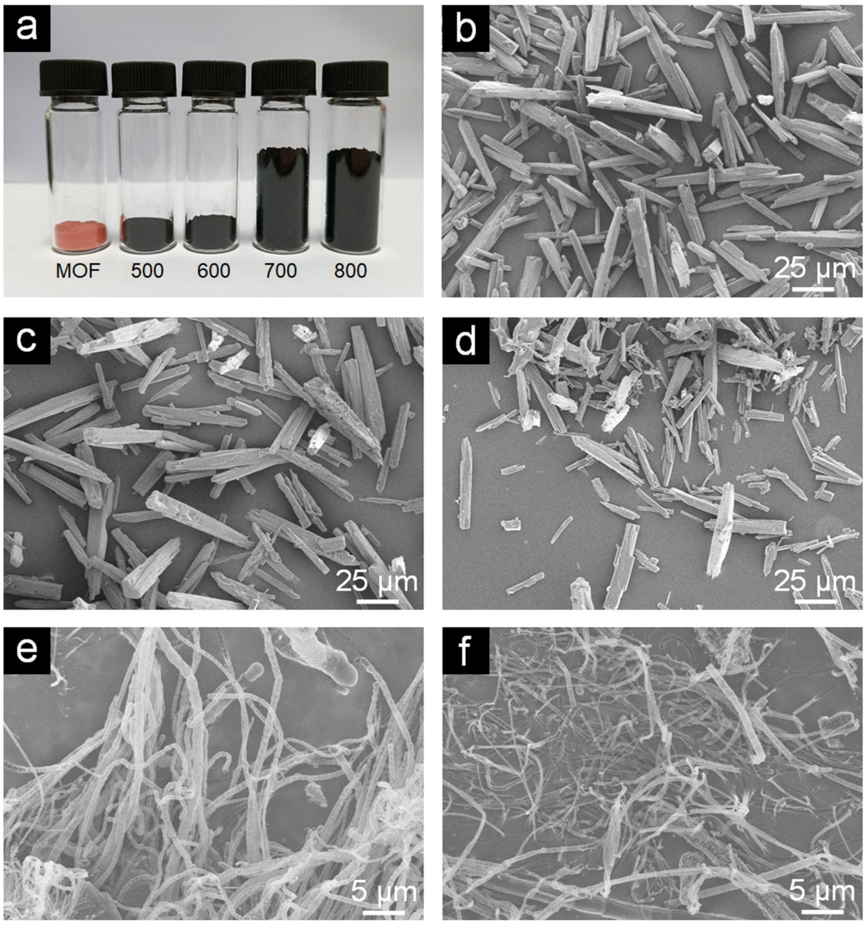

Fig. S4 (a) Photograph of Co-MOF and NC-*x* at the same mass. SEM images of (b) Co-MOF, (c) NC-500, (d) NC-600, (e) NC-700 and (f) NC-800 at a low magnification.

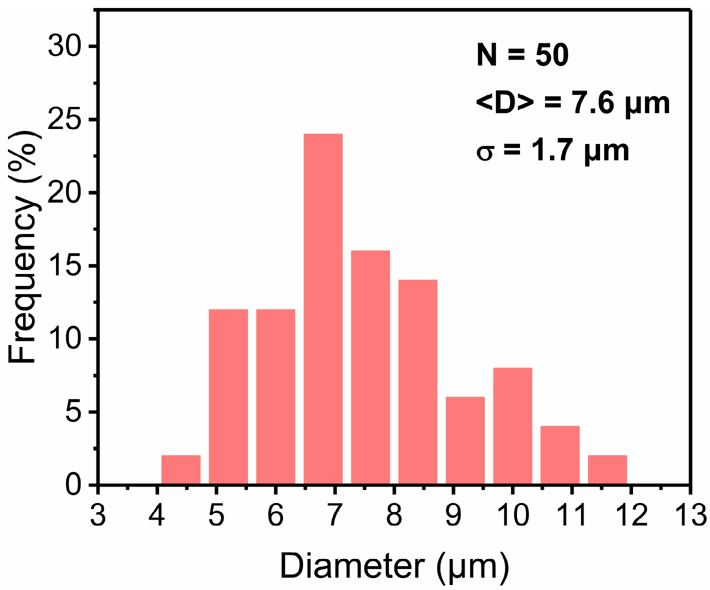

Fig. S5 The diameter distribution plot of Co-MOF. Note: N refers to the number of samples, <D> refers to the average diameter, and σ refers to the standard deviation.

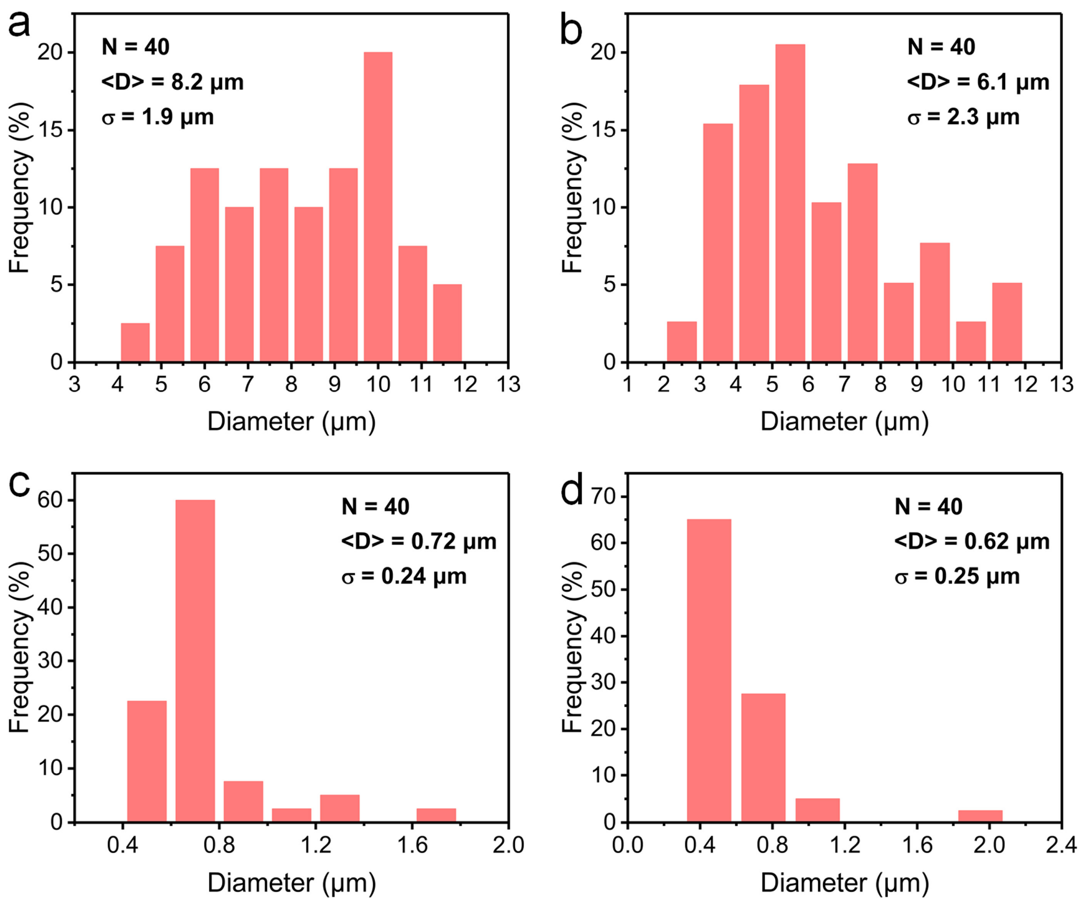

Fig. S6 Diameter distribution plots of (a) NC-500, (b) NC-600, (c) NC-700, and (d) NC-800. Note: N refers to the number of samples, <D> refers to the average diameter, and σ refers to the standard deviation.

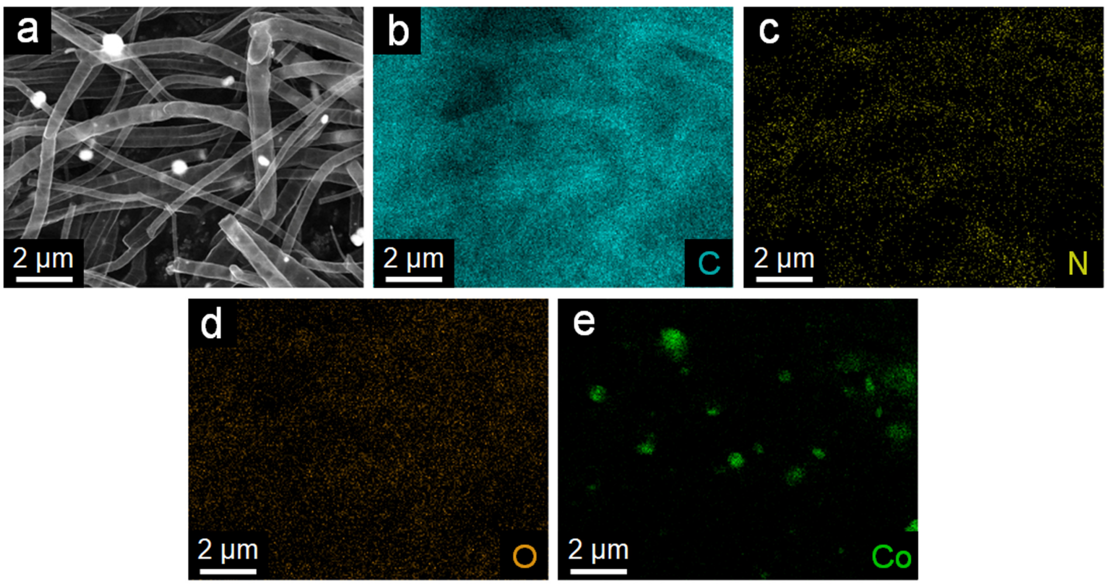

Fig. S7 (a) SEM image and (b-e) EDS maps of NC-700.

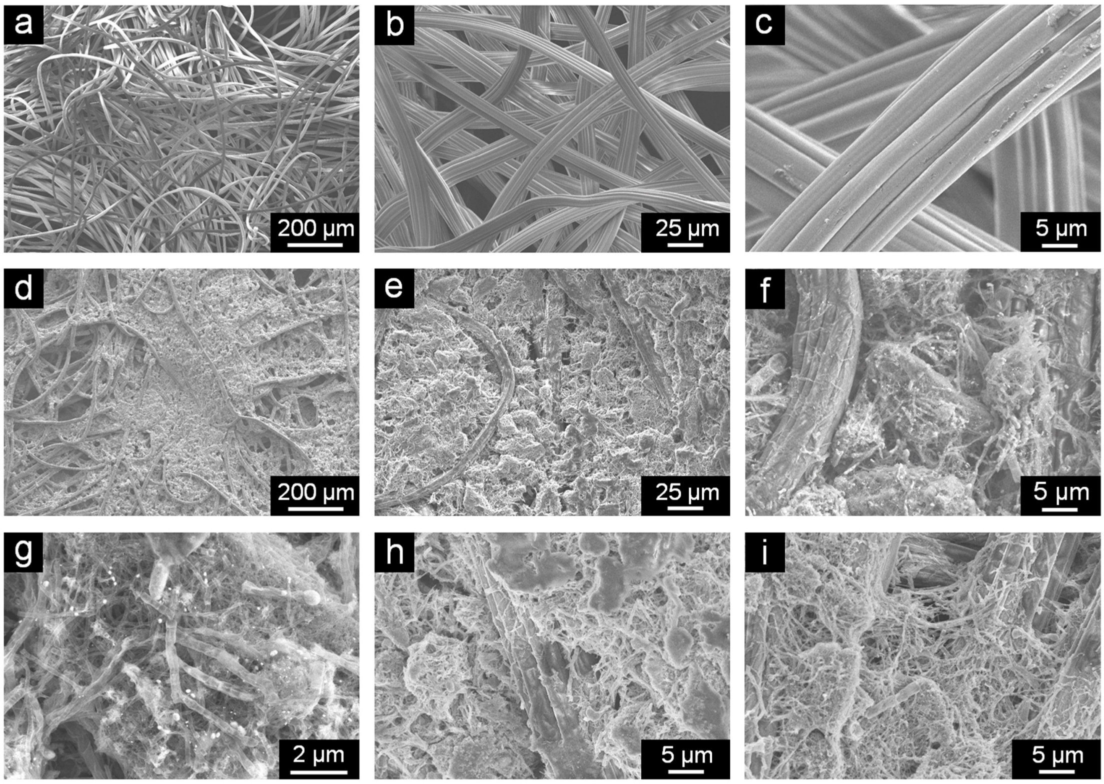

Fig. S8 SEM images of (a−c) non-woven cotton cloth, and (d−i) NC-700 coated cotton cloth.

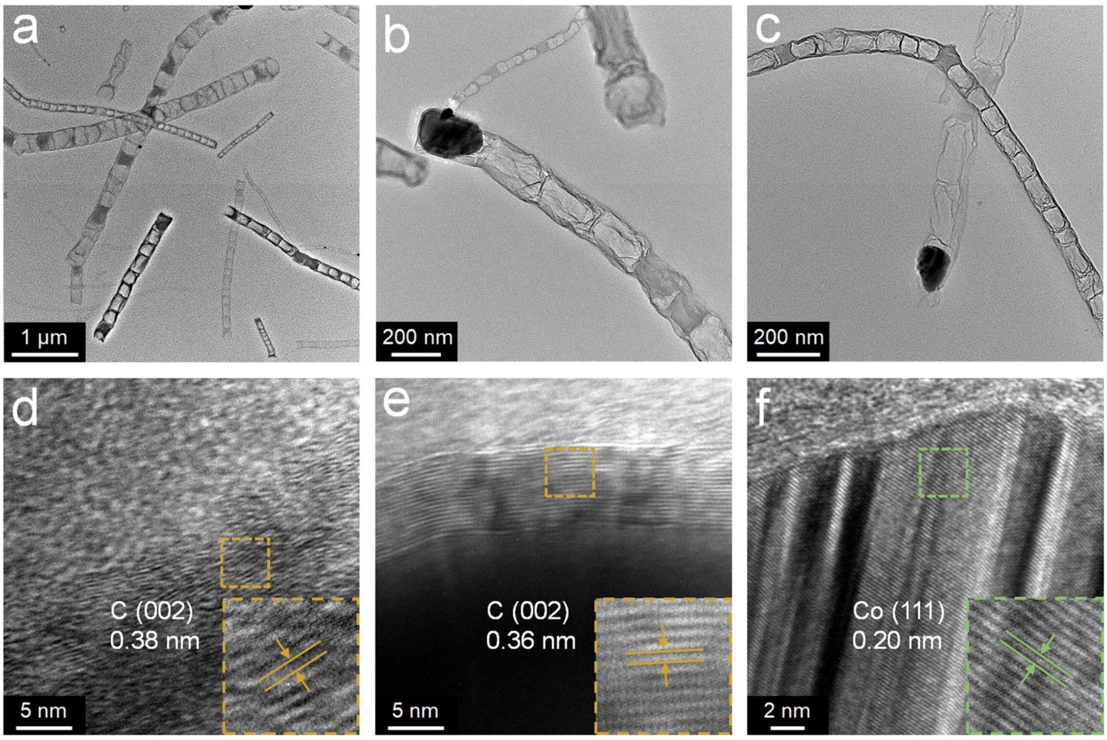

Fig. S9 (a−f) TEM images of NC-700 at low or high magnification.

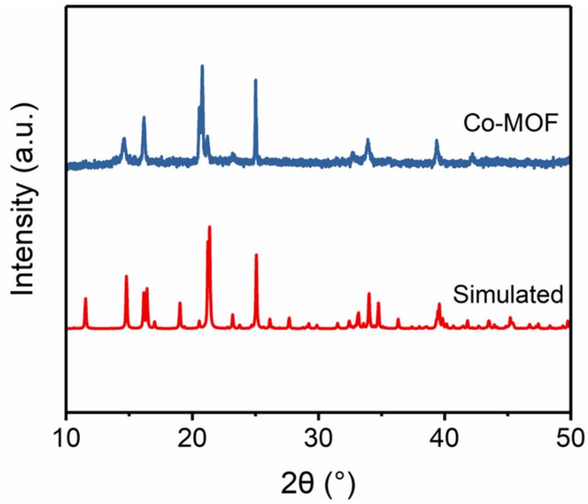

Fig. S10 XRD pattern of $Co(dca)_2pyz$, namely Co-MOF in this work.

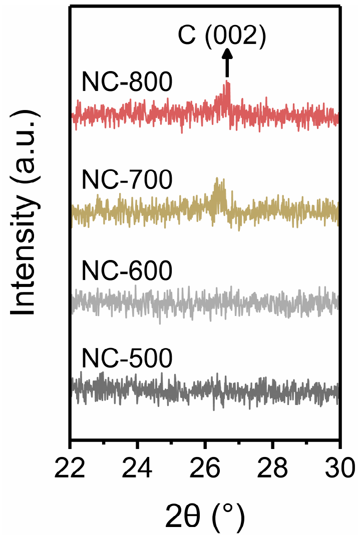

Fig. S11 XRD patterns of NC-*x* to show the weak diffraction peak (002) at ca. 26.6°.

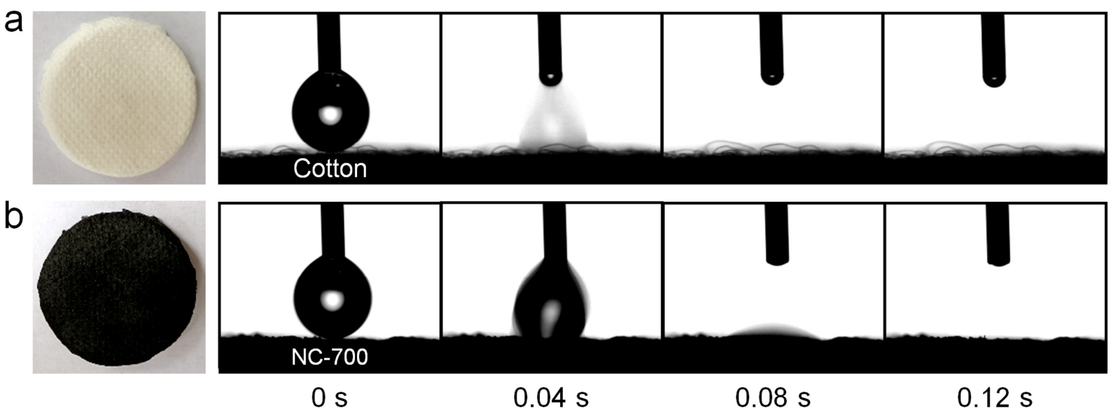

Fig. S12 Photographs and time evolution of the water contact angles of (a) cotton evaporator and (b) NC-700 evaporator.

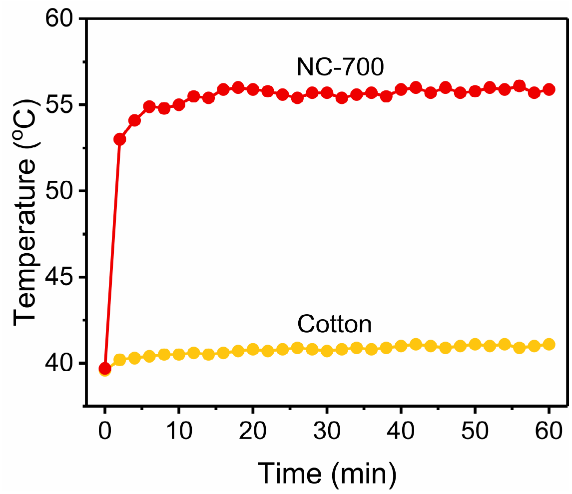

Fig. S13 Surface temperature curves of cotton evaporator and NC-700 evaporator in the wet state under 1 Sun irradiation.

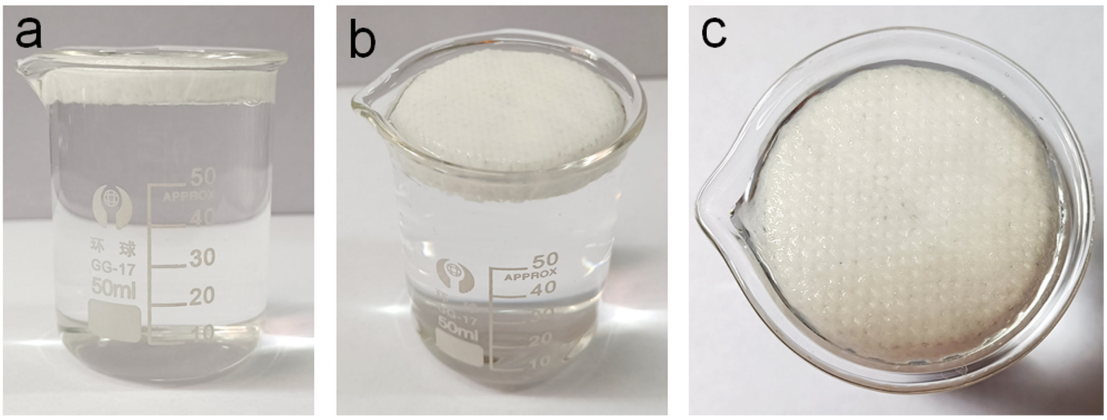

Fig. S14 (a-c) Photographs of the native cotton evaporator floating on the water.

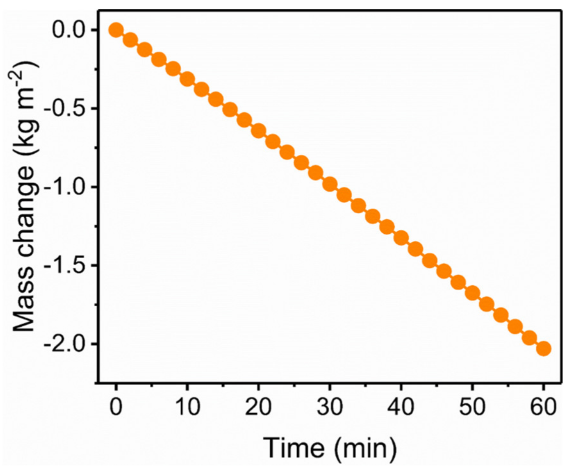

Fig. S15 Water mass change under 1 Sun irradiation using NC-700 evaporator after acid treatment to remove metallic cobalt.

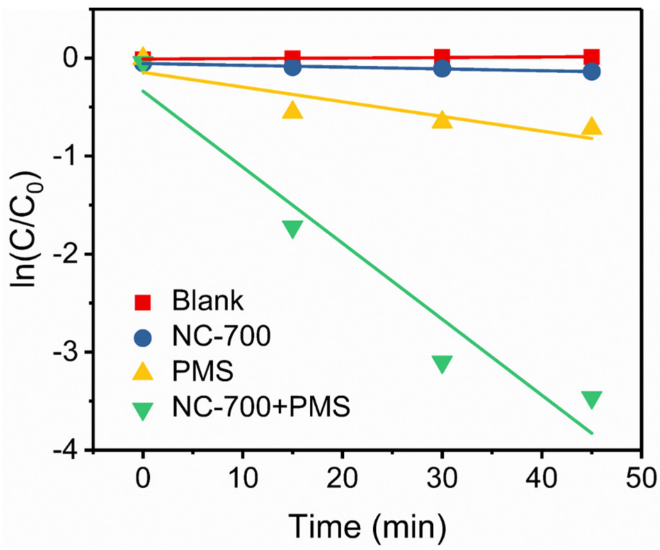

Fig. S16 The rate constant fitted curves in different conditions.

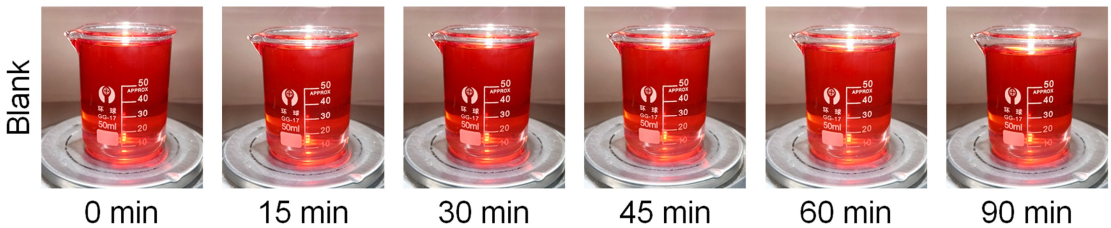

Fig. S17 Photographs showing the degradation of 100 ppm CR solution without NC-700 evaporator or PMS under 1 Sun irradiation.

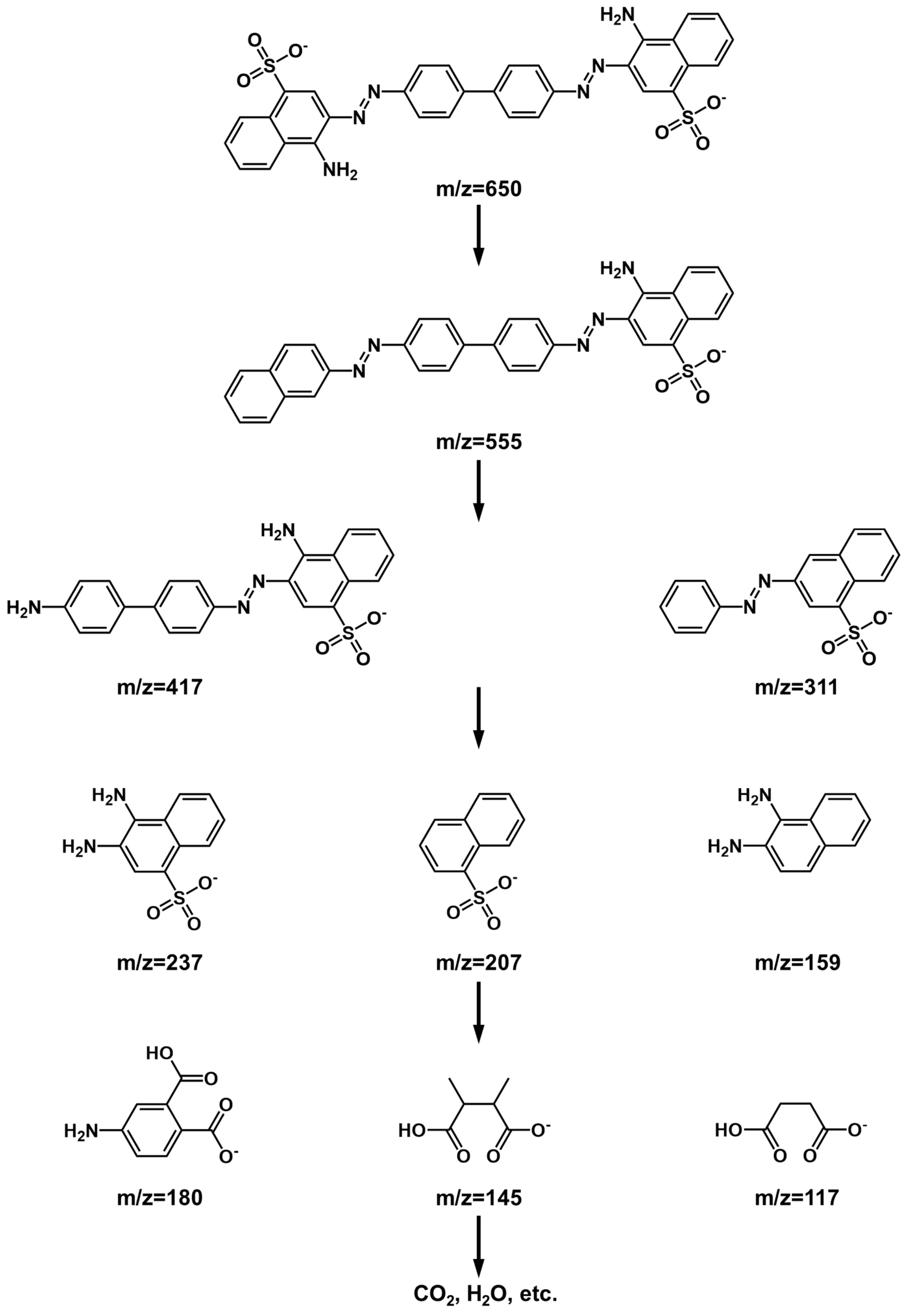

Fig. S18 Proposed degradation pathway of CR in the NC-700 + PMS system.

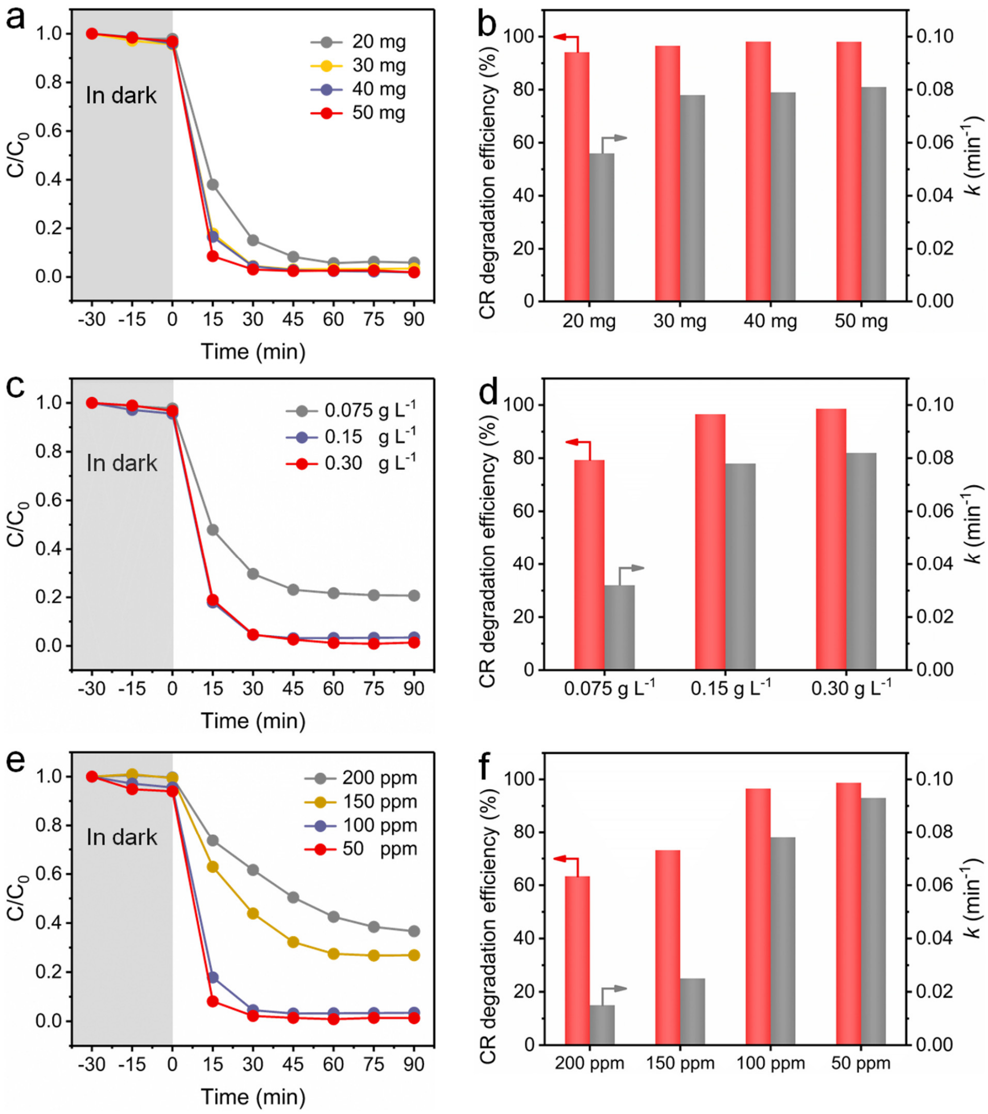

Fig. S19 The effects of (a and b) catalyst dosage, (c and d) PMS concentration, and (e and f) initial CR concentration on the degradation efficiency of CR and rate constant under NC-700 + PMS system.

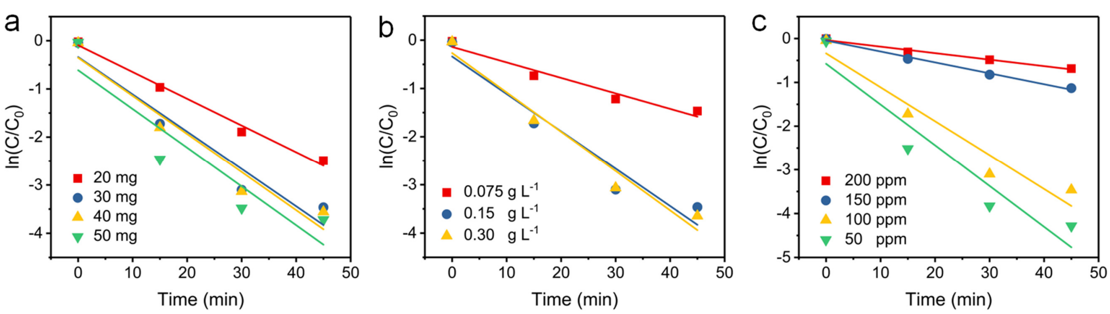

Fig. S20 The rate constant fitted curves of different (a) catalyst dosage, (b) PMS concentration, and (c) CR concentration.

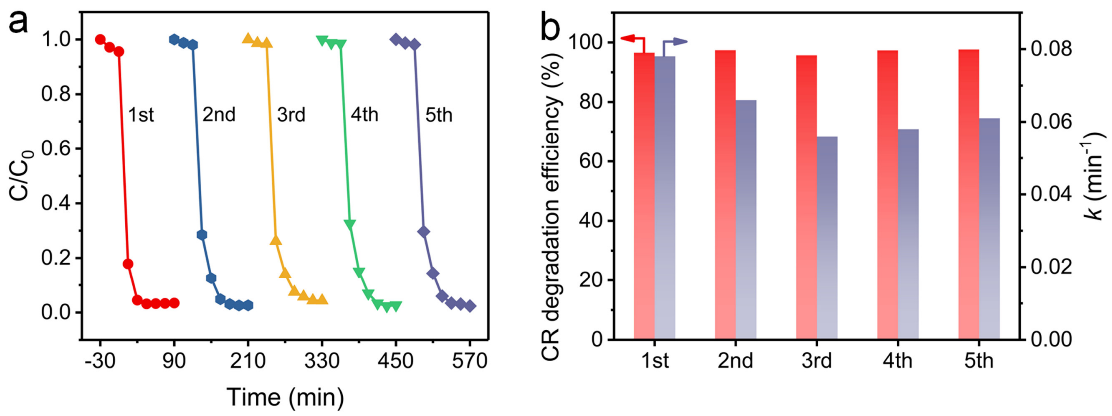

Fig. S21 (a) The degradation curves of CR using NC-700 + PMS system under visible light irradiation for 5 cycles. (b) Comparison of CR degradation efficiency and rate constant.

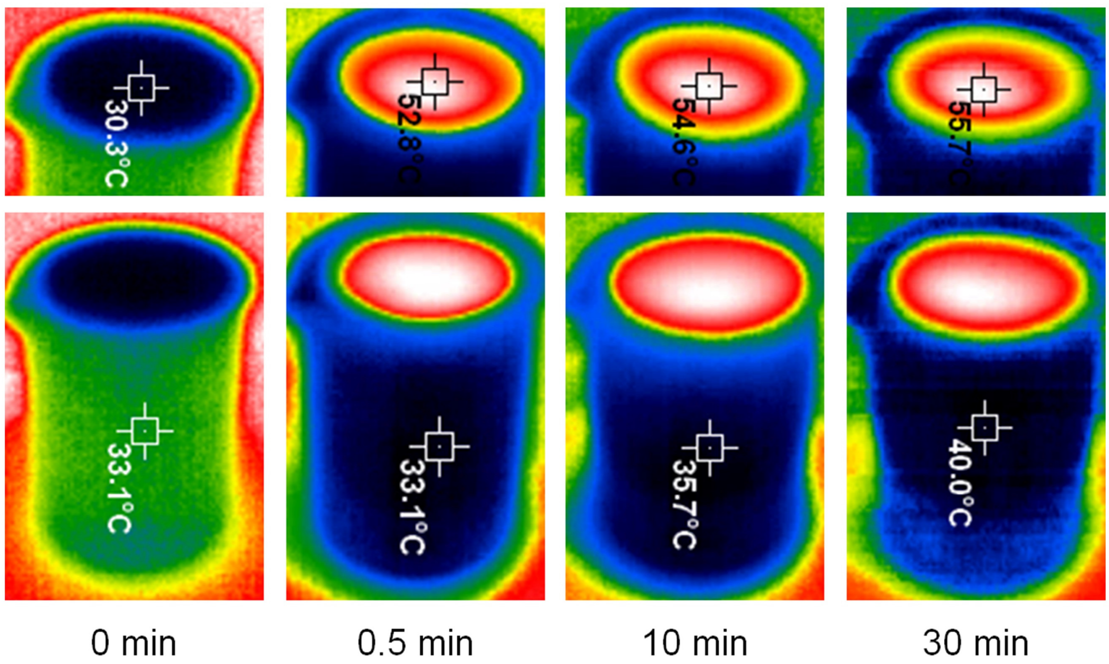

Fig. S22 Infrared images for the top surface or lateral surface of NC-700 evaporator floating on water under 1 Sun irradiation.

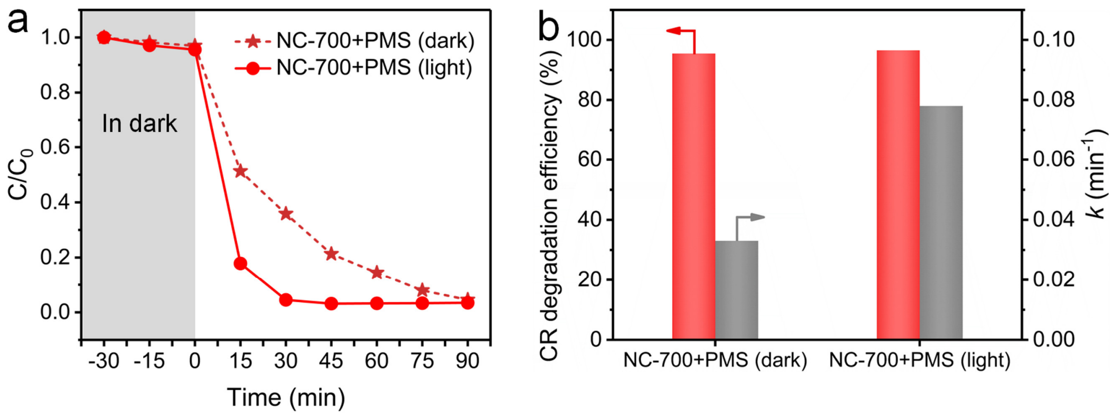

Fig. S23 (a) The degradation curves of CR using NC-700 + PMS system in the dark or under visible light irradiation. (b) Comparison of CR degradation efficiency and rate constant.

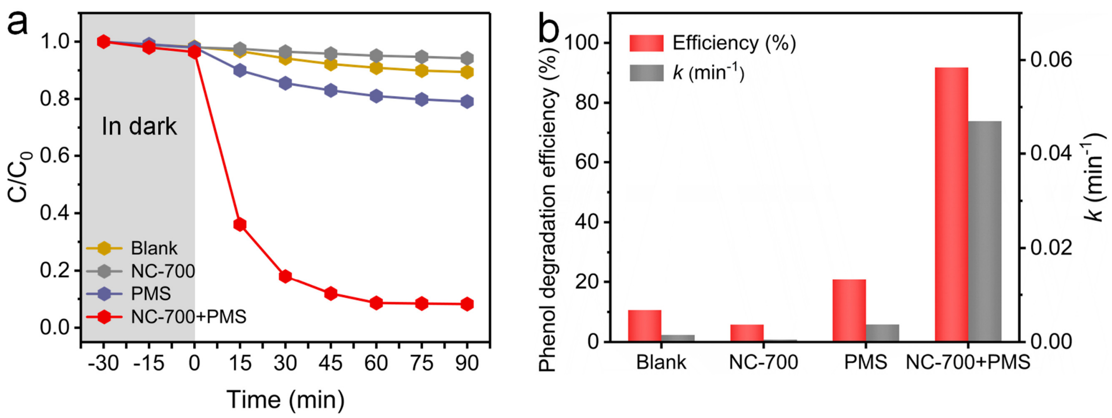

Fig. S24 (a) The degradation curves of phenol in different conditions under 1 kW m^{-2} irradiation. (b) Comparison of the corresponding degradation efficiency and rate constant of phenol (phenol solution = 30 ppm, 75 mL; NC-700 = 30 mg; PMS = 0.5 g L^{-1}).

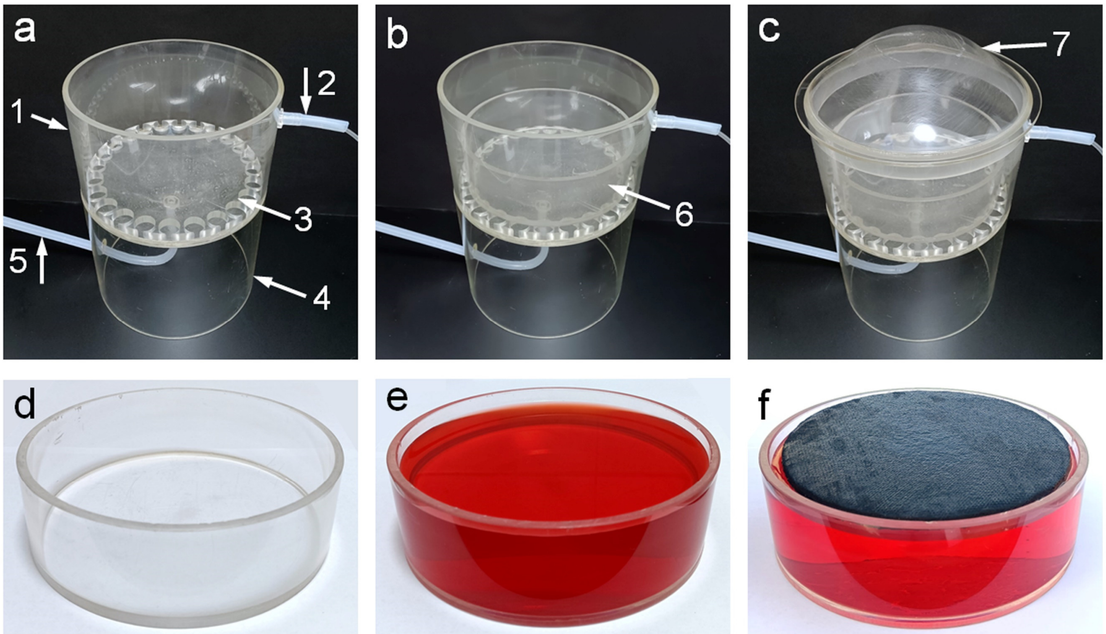

Fig. S25 (a−c) Photographs of the outdoor solar evaporation device without NC-700 evaporator. Photographs of (d) the container, (e) container with 1 L CR solution, and (f) container with CR solution and NC-700 evaporator. Note: 1−7 refer to the evaporation chamber (1), the upper pipe for collecting degraded solution (2), the supporting plate with edge holes (3), the support of evaporation chamber (4), the nether pipe for gathering condensed water (5), the container (6), and the vapor condenser (7).

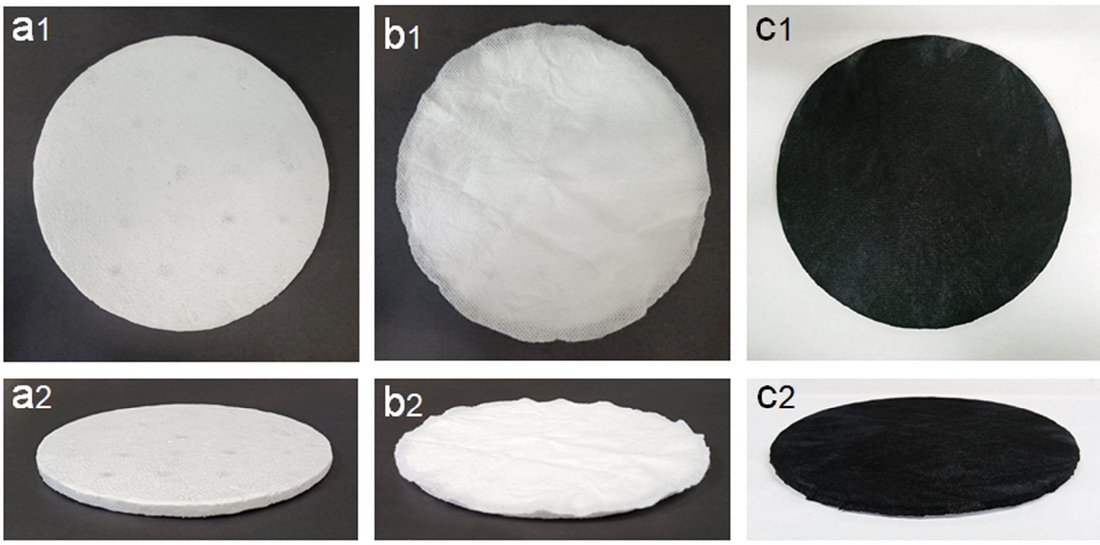

Fig. S26 Photographs of (a1 and a2) PS foam, (b1 and b2) cotton cloth covering PS foam, and (c1 and c2) NC-700 evaporator supported by PS foam.

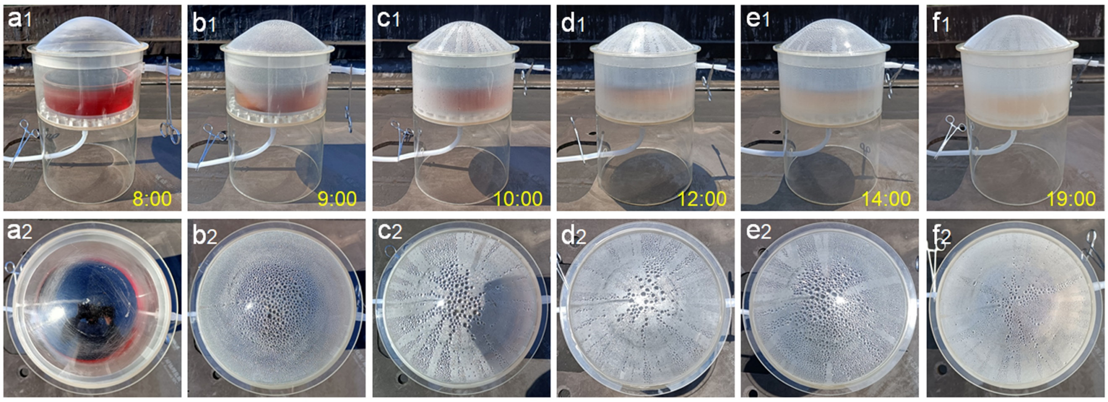

Fig. S27 Photographs of CR degradation and freshwater production progress in outdoor experiment.

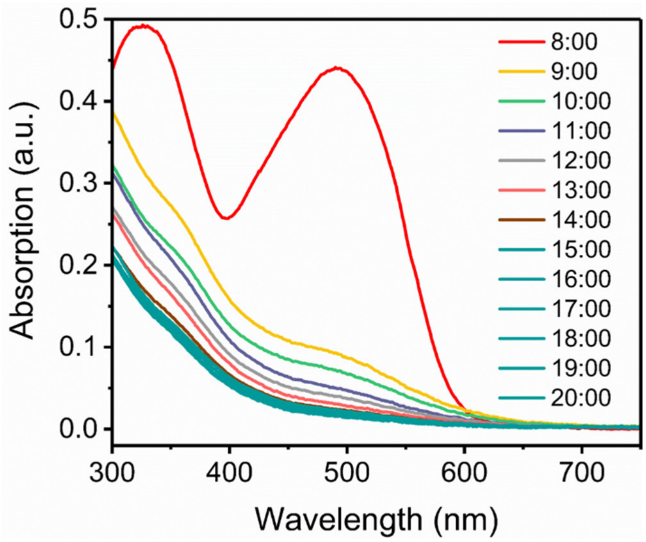

Fig. S28 UV-Vis absorption spectra of CR solution at different time in outdoor experiment.

Table S1 XPS analyses of Co-MOF and NC-*x* (*x* = 500, 600, 700 and 800).

Content (%)	Co-MOF	NC-500	NC-600	NC-700	NC-800
C	51.50	44.04	45.67	95.26	95.51
N	40.15	38.38	34.08	2.52	2.16
Co	5.42	7.20	8.15	0.25	0.26
O	2.93	10.38	12.10	1.97	2.07

Table S2 XPS chemical state analyses of Co-MOF and NC-x (x = 500, 600, 700 and 800).

Content (%)		Co-MOF	NC-500	NC-600	NC-700	NC-800
C 1s	C-C	28.5	27.9	33.6	58.4	56.5
	C-N	71.5	15.8	24.5	34.8	34.9
	N-C-O	-	56.3	41.9	6.8	8.6
N 1s	Pyridinic N	-	-	-	15.6	18.7
	Pyrrolic N	-	-	-	41.5	46.5
	Graphitic N	-	-	-	42.9	34.8
	N-Co	40.5	68.6	66.4	-	-
	N-C	59.5	31.4	33.6	-	-
Co 2p	Co^0	0	0	0~100	100	100
	Co^{2+}	100	100	100~0	0	0
O 1s	-C-O	-	62.6	69.1	66.3	67.8
	C-O-C	-	37.4	30.9	33.7	32.2

Table S3 Comparison of the solar vapor generation performance of NC-700 evaporator with some previous photothermal materials under 1 kW m^{-2} irradiation.

Entry	Photothermal material	Evaporation rate (kg m^{-2} h^{-1})	Efficiency (%)	Reference in ESI
1	NC-700	2.20	88.2	This work
2	PAN and PAN/GO bilayer membrane	2.27	92.6	[1]
3	Ag@PDA wooden flower	2.08	97	[2]
4	3D graphene network	1.64	91.8	[3]
5	RGO-SA-CNT aerogel	1.62	83	[4]

6	Snake-scale-like porous carbon	1.58	91	[5]
7	N-doped porous graphene	1.50	80	[6]
8	Carbonized mushroom	1.48	78	[7]
9	TiN/wood-derived carbon foam	1.47	92.5	[8]
10	Carbonized wood-slice	1.45	91.3	[9]
11	Aluminophosphate-treated wood	1.42	90.8	[10]
12	ALD/Chinese ink coated wood	1.31	82.2	[11]
13	Carbonized E. prolifera	1.3	84	[12]
14	TiO_2/nickel foam	1.25	78.5	[13]
15	Carbonized longitudinal wood	1.08	74	[14]
16	Carbonized moldy bread	0.96	71.4	[15]
17	Flexible wood membrane/CNT	0.95	65	[16]
18	rGO/cellous esters membrane	0.84	60	[17]
19	Au/disordered nanoporous template	0.80	64	[18]

Table S4 Comparison of the degradation performance of NC-700 by PMS activation with some previous carbon- or metal-based catalysts.

Entry	Catalyst	Pollutant	Degradation efficiency (%)	*k* (min^{-1})	PMS/catalyst [a]	Reference in ESI

1	NC-700	Congo red	96.6	0.078	0.375	This work
2	HCNFs	Tetracycline	80	0.075	2.5	[19]
3	PC-SC	Bisphenol A	95	0.072	1.5	[20]
4	ZIF-67/CNTs	Bisphenol A	96.8	0.096	0.1	[21]
5	Pt/Al_2O_3	Bisphenol A	100	0.096	0.61	[22]
6	NPC-800	Rhodamine b	85	0.043	7	[23]
7	MCCI	Rhodamine b	80	0.098	1	[24]
8	MCNC	Rhodamine b	90	0.301	5	[25]
9	Fe-N@C	Paracetamol	89.7	0.247	1.5	[26]
10	$CoN/N\text{-}C@SiO_2$	Tetracycline	98.6	0.247	0.4	[27]
11	NRGO	Sulfamethoxazole	91.7	0.010	0.49	[28]
12	$CoFe_2O_4$-EG	Sulfamethoxazole	99	0.265	0.2	[29]
13	CBs@NCCs-800	Methylene blue	97.6	0.1	16.7	[30]
14	PNC-800	Methylene blue	100	0.7	10	[31]
15	$MnFe_2O_4$/MS	Orange II	100	0.86	10	[32]

Note: ^{a} The activation efficiency of PMS, that is to say, the concentration ratio of the PMS to the catalyst. The low value of PMS/catalyst means the need of a relatively low amount of PMS when the content of catalyst keeps the same.

Table S5 Calculation for the cost of NC-700 evaporator.

Material	Cost	Remark
Pyrazine ($C_4H_4N_2$)	¥ 1.95/g	From Sinopharm Chemical Reagent Company
$Co(NO_3)_2·6H_2O$	¥ 0.87/g	
C_2H_5OH	¥ 0.02/mL	
C_2N_3Na	¥ 1.00/g	From Aladdin
PVA	¥ 0.03/g	From Kuraray
cotton cloth	¥ 3.63/m^2	From EAXAY
Co-MOF	¥ 3.7/g	In this process, 1.0 g $C_4H_4N_2$, 2.2 g C_2N_3Na and 3.5 g $Co(NO_3)_2·6H_2O$ are need to produce 2.2 g Co-MOF (the yield is about 66 %), and C_2H_5OH as detergent is required 50 mL.
NC-700	¥ 14.1/g	In this process, 2 g Co-MOF is pyrolyzed in tube finance under N_2 to produce 0.7 g NC-700 (the yield is about 35%). The cost for the electricity and equipment is estimated as ¥ 2.5.
NC-700 evaporator (Indoor test)	¥ 0.43/piece	In this process, 30 mg NC-700, a piece of cotton cloth (diameter=4.8 cm) and 1 mL PVA solution are needed. The cost for NC-700 evaporator is estimated as ¥ 0.43/piece.
NC-700 evaporator (Outdoor test)	¥ 7.5/piece	In this process, 530 mg NC-700, a piece of cotton cloth (diameter=17 cm) and 18 mL PVA solution are needed. The cost for NC-700 evaporator is estimated as ¥ 7.5/piece.

Note S1 Calculation of water evaporation enthalpy

The energy for water evaporation in the dark is obtained from the environment, which is same for different evaporators, according to the previous work [33-37]. Considering the known theoretical evaporation enthalpy value of liquid water (ca. 2.43 kJ g^{-1}), the water evaporation enthalpy values of cotton and NC-700 evaporator are calculated by the formula:

$$U_{in} = E_{equ} m_g = E_0 m_0 \tag{S1}$$

where U_{in} is the total energy absorbed from the environment per hour; E_0 and m_0 refer to the water evaporation enthalpy (2.43 kJ g^{-1}) and the mass change (g) in 1 h of water evaporation system (without evaporators) in dark condition, respectively; m_g means the water loss (g) of cotton and NC-700 evaporator, while E_{equ} is the equivalent evaporation enthalpy of corresponding system (kJ g^{-1}).

The water loss in darkness without solar evaporator or using PMS (i.e., cotton + PMS), NC-700 and NC-700+PMS is 243, 312, 354 and 351 mg, respectively. Hence, the water evaporation enthalpy of PMS, NC-700 and NC-700+PMS is calculated as 1.89, 1.67 and 1.68 kJ g^{-1}, respectively, lower than that of water (2.43 kJ g^{-1}). The water evaporation enthalpy of NC-700+PMS (1.68 kJ g^{-1}) is lower than that of PMS (cotton + PMS, 1.89 kJ g^{-1}), probably due to the hydrophilic group and porous structure of NC-700.

Note S2 Analysis of heat loss

Normally, the heat loss of water evaporation process includes radiation, convection and conduction. The calculation details of heat loss are shown as follows:

(1) Radiation

The radiation heat flux was calculated by the Stefan-Boltzmann equation:

$$\emptyset = \varepsilon A \sigma (T_1^4 - T_2^4) \tag{S2}$$

where $\emptyset$ represents heat flux, ε is the emissivity, and emissivity in the water evaporation processes is supposed as a maximum emissivity of 1. A is the effective evaporation surface area. σ is the Stefan-Boltzmann constant (the value is 5.67×10^{-8} W m^{-2} K^{-4}). T_1 is surface temperature of the as-prepared materials after stable steam generation under one-sun illumination (ca. 55 °C, 328.15 K), and T_2 is the ambient temperature (ca. 42 °C, 315.15 K).

Then, the radiation loss can be calculated by:

$$\eta_{rad} = \emptyset / P_{in} \tag{S3}$$

Under 1 kW m^{-2} irradiation, the radiation heat loss η_{rad} is calculated to be 9.8%.

(2) Convection

The convective heat loss is defined by Newton' law of cooling:

$$Q = hA\Delta T \tag{S4}$$

where Q is the the convection heat flux, h represents the convection heat transfer coefficient, which is approximately 5 W m^{-2} K^{-1}. ΔT is different between the surface temperature of NC-700 evaporator and the ambient temperature upward the absorber. Consequently, the connection heat loss of NC-700 was calculated through Equation S4, and the value is 6.5%.

(3) Conduction

$$Q = Cm\Delta T \tag{S5}$$

where Q is the heat energy, C represents the specific heat capacity of water (4.2 kJ K^{-1} kg^{-1}), and m denotes the weight of water (g). ΔT is the increased temperature of water. In this work, m = 70 g, ΔT = 0.5 K. Consequently, according to Equation S5, the calculated conduction heat loss of NC-700 is ca. 3.6%.

Therefore, the total heat loss of NC-700 in the water evaporation is ca. 19.9%.

References in ESI

1 L. Wang, C. Liu, H. Wang, Y. Xu, S. Ma, Y. Zhuang, W. Xu, W. Cui and H. Yang, *ACS Appl. Mater. Interfaces*, 2020, **12**, 24328-24338.

2 S. Chen, Z. Sun, W. Xiang, C. Shen, Z. Wang, X. Jia, J. Sun and C. J. Liu, *Nano Energy*, 2020, **76**, 104998.

3 K. Kim, S. Yu, C. An, S. W. Kim and J. H. Jang, *ACS Appl. Mater. Interfaces*, 2018, **10**, 15602-15608.

4 X. Hu, W. Xu, L. Zhou, Y. Tan, Y. Wang, S. Zhu and J. Zhu, *Adv. Mater.*, 2017, **29**,

1604031.

5 N. Liu, L. Hao, B. Zhang, R. Niu, J. Gong and T. Tang, *Sustain. Energ. Fuels*, 2020, **4**, 5522-5532.

6 Y. Ito, Y. Tanabe, J. Han, T. Fujita, K. Tanigaki and M. Chen, *Adv. Mater.*, 2015, **27**, 4302-4307.

7 N. Xu, X. Hu, W. Xu, X. Li, L. Zhou, S. Zhu and J. Zhu, *Adv. Mater.*, 2017, **29**, 1606762.

8 D. Guo and X. Yang, *Sci. China Mater.*, 2019, **62**, 711-718.

9 P. F. Liu, L. Miao, Z. Deng, J. Zhou, H. Su, L. Sun, S. Tanemura, W. Cao, F. Jiang and L. D. Zhao, *Mater. Today Energy*, 2018, **8**, 166-173.

10 T. Chen, Z. Wu, Z. Liu, J. T. Aladejana, X. A. Wang, M. Niu, Q. Wei and Y. Xie, *ACS Appl. Mater. Interfaces*, 2020, **12**, 19511-19518.

11 H. C. Yang, Z. Chen, Y. Xie, J. Wang, J. W. Elam, W. Li and S. B. Darling, *Adv. Mater. Interfaces*, 2019, **6**, 1801252.

12 L. Yang, G. Chen, N. Zhang, Y. Xu and X. Xu, *ACS Sustainable Chem. Eng.*, 2019, **7**, 19311-19320.

13 X. Chen, C. Meng, Y. Wang, Q. Zhao, Y. Li, X. M. Chen, D. Yang, Y. Li and Y. Zhou, *ACS Sustainable Chem. Eng.*, 2020, **8**, 1095-1101.

14 H. Liu, C. Chen, G. Chen, Y. Kuang, X. Zhao, J. Song, C. Jia, X. Xu, E. Hitz, H. Xie, S. Wang, F. Jiang, T. Li, Y. Li, A. Gong, R. Yang, S. Das and L. Hu, *Adv. Energy Mater.*, 2018, **8**, 1701616.

15 Y. Zhang, S. K. Ravi, J. V. Vaghasiya and S. C. Tan, *iScience*, 2018, **3**, 31-39.

16 C. Chen, Y. Li, J. Song, Z. Yang, Y. Kuang, E. Hitz, C. Jia, A. Gong, F. Jiang, J. Y. Zhu, B. Yang, J. Xie and L. Hu, *Adv. Mater.*, 2017, **29**, 1701756.

17 G. Wang, Y. Fu, X. Ma, W. Pi, D. Liu and X. Wang, *Carbon*, 2017, **114**, 117-124.

18 L. Zhou, Y. Tan, D. Ji, B. Zhu, P. Zhang, J. Xu, Q. Gan, Z. Yu and J. Zhu, *Sci. Adv.*, 2016, **2**, e1501227.

19 C. Wang, J. Kim, M. Kim, H. Lim, M. Zhang, J. You, J. H. Yun, Y. Bando, J. Li and Y. Yamauchi, *J. Mater. Chem. A*, 2019, **7**, 13743-13750.

20 W. D. Oh, A. Veksha, X. Chen, R. Adnan, J. W. Lim, K. H. Leong and T. T. Lim, *Chem. Eng. J.*, 2019, **374**, 947-957.

21 J. Ye, C. Li, L. Wang, Y. Yan, Y. Wang and J. Dai, *Sep. Purif. Technol.*, 2021, **258**, 117669.

22 Y. Wang, S. Hui, S. Zhan, R. Djellabi, J. Li and X. Zhao, *Chem. Eng. J.*, 2020, **381**, 122563.

23 W. Ma, Y. Du, N. Wang and P. Miao, *Environ. Sci. Pollut. Res.*, 2017, **24**, 16276-16288.

24 K. Y. A. Lin and B. J. Chen, *Chemosphere*, 2017, **166**, 146-156.

25 C. H. Wu, J. T. Lin and K. Y. A. Lin, *J. Colloid Interface Sci.*, 2018, **517**, 124-133.

26 C. Chen, T. Ma, Y. Shang, B. Gao, B. Jin, H. Dan, Q. Li, Q. Yue, Y. Li, Y. Wang and X. Xu, *Appl. Catal. B-Environ.*, 2019, **250**, 382-395.

27 S. Zhang, H. Gao, X. Xu, R. Cao, H. Yang, X. Xu and J. Li, *Chem. Eng. J.*, 2020, **381**, 122670.

28 S. Wang, L. Xu and J. Wang, *Chem. Eng. J.*, 2019, **375**, 122041.

29 M. Xu, J. Li, Y. Yan, X. Zhao, J. Yan, Y. Zhang, B. Lai, X. Chen and L. Song, *Chem. Eng. J.*, 2019, **369**, 403-413.

30 N. Wang, W. Ma, Z. Ren, L. Zhang, R. Qiang, K. Y. A. Lin, P. Xu, Y. Du and X. Han, *Inorg. Chem. Front.*, 2018, **5**, 1849-1860.

31 N. Wang, W. Ma, Z. Ren, Y. Du, P. Xu and X. Han, *J. Mater. Chem. A*, 2018, **6**, 884-895.

32 H. Fu, S. Ma, P. Zhao, S. Xu and S. Zhan, *Chem. Eng. J.*, 2019, **360**, 157-170.

33 X. Zhou, Y. Guo, F. Zhao, W. Shi and G. Yu, *Adv. Mater.*, 2020, **32**, 2007012.

34 Y. Sekine and T. Ikeda-Fukazawa, *J. Chem. Phys.*, 2009, **130**, 034501.

35 Y. Guo, H. Lu, F. Zhao, X. Zhou, W. Shi and G. Yu, *Adv. Mater.*, 2020, **32**, 1907061.

36 F. Zhao, Y. Guo, X. Zhou, W. Shi and G. Yu, *Nat. Rev. Mater.*, 2020, **5**, 388-401.

37 X. Zhou, F. Zhao, Y. Guo, B. Rosenberger and G. Yu, *Sci. Adv.*, 2019, **5**, eaaw5484.